JOINT EUROPEAN TORUS JET

JET–P(93)68

S.V. Putvinskii, B.J.D. Tubbing, L-G. Eriksson, S.V. Konovalov

On the Modelling of Fast Particle Ripple Losses in Tokamaks

Neutron Emission Profile Measurements during the First Tritium Experiments at JET

S.V. Putvinskii[1], B.J.D. Tubbing, L-G. Eriksson, S.V. Konovalov

JET-Joint Undertaking, Culham Science Centre, OX14 3DB, Abingdon, UK

[1]Present address: ITER US co-centre, San Diego, USA.
[2]I.V.Kurchatov Inst. Moscow, Russia

Preprint of a paper to be submitted for publication in
Nuclear Fusion
September 1993

ABSTRACT

The Bounce Average Fokker-Plank equation describing fast particles in a tokamak with toroidal magnetic field ripple has been solved numerically by a Monte-Carlo approach. The essential element is that the ripple effect is treated as a diffusion of banana trapped particles. The diffusion coefficient is pre-calculated from a semi-analytical expression for a given plasma geometry. The kinetic equation is solved for the processes of fast particle slowing down, pitch angle scattering, ripple diffusion and acceleration by ion cyclotron resonance heating. This approach was found particularly useful for the study of fast particle behavior in non-stationary conditions, including sawtooth effects. A ripple loss code has been developed on the basis of this principle. The code has been benchmarked against a full Orbit Following Monte Carlo code. Applications of the code to experimental results from the JET experiments with 16 vs 32 toroidal field coils are shown.

1. INTRODUCTION

The analysis of high energy particle confinement in a tokamak with 3D perturbations of the magnetic field is usually a difficult task because of the large number of essential phase variables. A traditional problem for tokamak reactor studies is the evaluation of fast particle losses (alpha-particles in reactors) caused by toroidal field ripple. The toroidal field ripple arises from the discreteness of the toroidal coils. The ripple loss of fusion alpha-particles, with the associated heat loads on first wall and in-vessel components, is acknowledged to be the major limitation on the permissible amplitude of the ripple in a tokamak reactor, thereby setting a lower limit on the number of coils.

Traditionally, fast particle losses have been studied with the aid of Orbit Following Monte-Carlo Codes (OFMC) [1,2,3]. These codes evaluate fast particle losses by calculating slowing down histories of large number of individual particles moving in 3D magnetic fields, following their guiding centers. This approach is useful for modeling of high energy ions in a general magnetic field structure, but has very limited application because extremely large computer run times are required.

Simplified codes [4,5] have been developed to obtain a fast estimate of the ripple loss in tokamaks. In particular, in the code RIPLOS [5] it is assumed that all

particles born within the 'stochastic diffusion region' are immediately lost from the plasma while all other particles are confined. Although this approach provides reasonable estimates of the total ripple loss fraction, detailed information about fast particle distribution functions can not be obtained.

The JET experiments with reduced number of TF coils [6,7] highlighted the need for an intermediate level of treatment of fast particle ripple losses. A significant number of discharges needed to be analysed, time-dependently, for three classes of fast particles: particles produced by Neutral Beam (NB) Injection, minority ions accelerated by Ion Cyclotron Resonance Heating (ICRH) and tritons born in D-D fusion reactions. It was clear that the use of an OFMC would be too time consuming for this work.

The present treatment is based on the observation [8] that the effect of small toroidal field ripple on the fast particle distribution function can be described by a spatial diffusion. The diffusion rate can be evaluated as a function of local plasma parameters, ripple value and particle parameters averaged over the particle bounce period [6]. Therefore, a Bounce Average Fokker-Plank kinetic equation (BAFP) with an additional ripple operator provides an adequate description of the problem. In the present paper we apply a statistical - or Monte-Carlo - method for the solution of the problem in this form.

The solution of the BAFP equation by a Monte-Carlo technique is found by calculating the time histories of particle coordinates, which are invariants of the unperturbed motion, for a large number of test particle random orbits. For example, for banana particles, such coordinates are particle velocity, and radial and vertical banana tip position. The Langevin equations which describe single particle random motion in these coordinates can be straightforwardly derived from the particular form of the BAFP equation. The time step for numerical integration of the Langevin equations in the presence of ripple diffusion can be of the order of $\Delta t = \Delta x^2 / D_{rip}$, where Δx is a typical spatial integration stepsize set to a small fraction of the minor radius, and D_{rip} is the ripple diffusion coefficient. Typical values for Δt are between 10^{-3} and 10^{-5}s. This should be compared with OFMC codes, which must integrate with a time step of the order of a small fraction of the bounce time, i.e. of the order of 10^{-7} to 10^{-8}s. Thus, the use of the Bounce Average procedure gives a large gain in computer run time in comparison with OFMC's, for the same statistical accuracy.

The statistical or Monte-Carlo method is known to be particularly useful for the solution of multi-dimensional problems. It allows a description which corresponds to the actual plasma geometry and magnetic field structure and is flexible to the inclusion of additional physical effects. It is furthermore particularly useful for the study of particle behavior in non-stationary conditions. A new code, RLX-1, was therefore developed, based on the method outilined above, i.e. the Monte Carlo solution of the 3-dimensional, time-dependent BAFP equation. Physics effects included in the code are slowing down, pitch angle scattering, stochastic ripple diffusion, acceleration by ICRH fields, sawteeth, and time-dependent background plasma parameters. The main approximations are the use of the small larmor radius approximation, and the use of the analytical expression given in [6] for the stochastic ripple diffusion coefficient. Neither of these approximations are essential to the method. In particular, the semi-analytical expression can be replaced by a diffusion coefficient 'map' directly obtained via numerical cloud-spreading experiments with an OFMC.

Section 2 of the paper is devoted to the formulation of the problem and a description of the method. Benchmark comparisons of the newly developed code RLX-1 with results of a full OFMC are presented in Section 3. In section 4, results of simulations of the JET experiments with 16 versus 32 coils are presented.

2. FORMULATION OF THE PROBLEM

The evolution of the fast particle distribution function $f(\underline{R},\underline{v},t)$, on time scales larger than the particle bounce time, τ_b, can be described by the BAFP kinetic equation [9]. This equation can be written as follows:

$$\frac{\partial f}{\partial t} = S(f) + L_{ripp}(f) + L_{RF}(f) + L_{ST}(f) + \langle S \rangle \qquad (1)$$

where S(f) is the Coulomb collisional term, L_{rip} (f) is the operator which describes the ripple diffusion, L_{RF} (f) is the term representing particle interaction with the ICRH field, L_{ST}(f) is the operator describing particle mixing during sawtooth crashes, and <S> is a particle source averaged over the bounce period. The different terms are discussed in the following sections. In the evaluation of these terms the zero banana-width approximation will be adopted (although that is not a fundamental restriction of the method).

2.1 Coulomb collisions

The coordinates for the formulation of the Coulomb operator are v, a, λ, where v is particle velocity, a is the normalised minor radius in the low field side (LFS) horizontal midplane (used as a flux surface label), and λ is a pitch angle parameter such that $\lambda = (v_{//0} / v)^2$, where $v_{//0}$ is the parallel velocity at the LFS midplane ($\theta = 0$). This choice of coordinates is natural because to first order collisional processes affect only v and λ, while a is conserved. We shall keep only the leading terms in the collision operator which correspond to the fast particle slowing down on the background plasma and scattering on the plasma ions:

$$S(f) = \frac{1}{G_{v,a,\lambda}} \frac{\partial}{\partial v} \left[G_{v,a,\lambda} \; U_{slo} \; f \right] + \frac{1}{G_{v,a,\lambda}} \frac{\partial}{\partial \lambda} \left[G_{v,a,\lambda} \; D_{pas} \; \frac{\partial f}{\partial \lambda} \right] \tag{2}$$

in which $G_{v,a,\lambda}$ is the jacobian for the v,a,λ coordinates, U_{slo} is the slowing down coefficient and D_{pas} is the pitch angle scattering diffusion coefficient:

$$U_{slo} = \frac{v}{\tau_s} \left(1 + \frac{v^{*3}}{v^3} \right)$$

$$D_{pas} = \frac{2}{\tau_s} \frac{v^{**3}}{v^3} \lambda \left(1 - \lambda \right) F(\lambda)$$

in which τ_s is the slowing down time, and v* and v** are critical velocities for slowing down and pitch angle scattering, respectively, and F is a geometrical function:

$$\tau_s(a) = \frac{3}{8 \sqrt{2\pi}} \frac{m_\alpha}{\sqrt{m_e}} \frac{T_e^{3/2}}{\lambda_e \; e^4 \; Z_\alpha^2 \; n_e}$$

$$v^*(a) = \left(\frac{3 \sqrt{\pi} \; \lambda_i \; m_e}{4 \; \lambda_e \; n_e} \sum_\beta \frac{Z_\beta^2 \; n_\beta}{m_\beta} \right)^{1/3}$$

$$v^{**}(a) = \left(\frac{3 \sqrt{\pi} \; \lambda_i \; m_e}{4 \; \lambda_e \; n_e} \sum_\beta \frac{Z_\beta^2 \; n_\beta}{m_\alpha} \right)^{1/3}$$

$$F(\lambda) = \left(< R / R_{LF} > - 1 + \lambda \right) \frac{1}{\lambda}$$

where subscripts α, β, e refer to mass and charge for the fast ion species, the plasma ion species (incl. impurities) and electrons, respectively, λ_e and λ_i are Coulomb logarithms for electrons and ions, T_e, n_e are electron temperature and density, R_{LF} is the LFS midplane major radius ($\theta = 0$) of the flux surface, R_0 is the radius of the magnetic axis and <..> implies the bounce average:

$$<..> = \frac{1}{\tau_B} \int_0^{\tau_B} (..)\, dt$$

The jacobian for the coordinate system v,a,λ is:

$$G_{v,a,\lambda} = \frac{\tau_B \; v^3 \; R_{LF}}{4\pi \; R_0 \; B_0} \frac{\partial \; \Psi}{\partial \; a} * \begin{pmatrix} 1 & \text{for transit particles} \\ 0.5 & \text{for banana particles} \end{pmatrix} \quad (3)$$

where Ψ is the poloidal flux.
The difference in the factor two between transit and banana particles originates from the definition of the bounce time:

$$\tau_B = \int_{-\pi}^{\pi} \frac{dl}{v_{//}} \text{ for transit and } \tau_B = 2 \int_{-\theta_B}^{\theta_B} \frac{dl}{v_{//}} \text{ for banana particles.} \quad (4)$$

where θ_B is the poloidal bounce angle (midplane to bounce point).

2.2 Ripple diffusion

We consider here only plasmas that are vertically symmetric around the midplane. Furthermore, transit particles are assumed not to be affected by the ripple. They can only be lost through Coulomb scattering into banana particles.

The plasma cross-section can be divided in two different regions. The boundary between the regions is given by $\nu = 1$, where the ripple parameter is given by $\nu = B\ N\ \delta\ /\ B_R$. Here $\delta = (B_{max} - B_{min})/(B_{max} + B_{min})$ is the amplitude of the ripple, N is the number of TF coils, B is the total magnetic field and B_R is the radial component of the poloidal magnetic field.

The ripple well region, $\nu > 1$,exists at the low field side, and near the plasma boundary If the turning point of a banana orbit is located in the ripple well region the particle can be trapped in the magnetic well [10]. A ripple-well trapped particle will drift vertically due to vertical drifts (grad B and curvature drift). Its further destination is defined by the dependence of the well depth on the vertical coordinate. In the upper part of the plasma cross section, i.e. above a certain

critical z value, $\partial\nu / \partial z > 0$, i.e. the well depth increase with the vertical coordinate z. A particle being trapped there becomes more deeply trapped and is lost to the first wall. For particle energies exceeding several tens of keV the probability of trapping is very high and we consider the region $\nu > 1$, $\partial\nu / \partial z > 0$ as an instant loss-cone. In the region $\nu > 1$, $\partial\nu / \partial z < 0$, the ripple well depth decreases as the particle drifts vertically, and the particle will de-trap. Such particles are not considered lost, but are in general subject to strong stochastic diffusion.

In the remainder of the plasma cross section (where there are no ripple wells) the TF ripple leads to spatial diffusion of banana particles [6]. Because the particle magnetic moment remains constant the ripple diffusion corresponds to a displacement of the banana turning points along lines with B = const or approximately vertical lines with R = const. This effect is described by the second term on the right hand side of equation 1. We formulate the ripple diffusion (which affects only banana particles) in cylindrical coordinates of the banana bounce point, R_B, z_B. This choice is natural because under the ripple operator z_B is affected while R_B is conserved, so that a one dimensional diffusion results. Then the operator is:

$$L_{rip}(f) = \frac{1}{G_{R,z}} \frac{\partial}{\partial z_B} \left(G_{R,z} \; D_{rip} \; \frac{\partial f}{\partial z_B} \right) \tag{5}$$

where $G_{R,z}$ is the jacobian for the R_B, z_B coordinates, and D_{rip} is the ripple diffusion coefficient, which can be found in the review [6].

$$D_{rip} = \frac{\Delta z_B^2}{\tau_B} \; I_W \tag{6}$$

where Δz_b is the vertical step in the bounce point due to the ripple field, and I_W is a function representing the de-correlation between steps in successive bounces.

$$\Delta z = \rho_L \left(\frac{\pi}{N} \right)^{1/2} \left(\frac{B}{B_R} \right)^{1/2} \frac{\nu}{1 + \nu^{3/2} / \pi^{1/2}} \tag{7}$$

I_W consists of two terms, the first representing collisional de-correlation, the second representing stochastic diffusion:

$$I_W = \frac{1 - e^{-4\eta}}{\left(1 - e^{-2\eta}\right)^2 + 4 \; e^{-2\eta} \left(\sin^2 (N\varphi_P) + 0.46\gamma^2 \right)} + \frac{1}{1 + e^{(6.9 - 5.5\gamma)}} \tag{8}$$

where the toroidal precession angle φ_P, the Chirikov parameter γ, and η are given by:

$$\varphi_P = \frac{\pi \; v^2 \; m_\alpha}{Z_\alpha} \; \frac{\partial}{\partial \Psi} \left(\tau_B \; \left(1 - \left(1 - \lambda\right)\right) \; < R_{LF} / R > \right)$$

$$\eta = \frac{\tau_B}{\tau_{ii}} \; \frac{N^2 \; q^2 \; R_B^2}{R_{LF}^2} \; \frac{\left(1 - \left(1 - \lambda\right) < R_{LF} / R >\right)}{\lambda \; \left(\lambda_{cr} - \lambda\right)}$$

$$\gamma = \Delta z_B \; N \; \frac{\partial \varphi_B}{\partial z_B}$$

where τ_{ii} is the ion-ion collision time, q is the safety factor, λ_{cr} is the critical value of λ, i.e. the value at the trapped / transit boundary, and φ_B is the toroidal bounce angle, i.e. the toroidal angle of the banana tip with respect to the angle of the midplane point of the orbit.

The Jacobian for the R_B, z_B coordinates is (note the velocity factor is not included because it is not needed):

$$G_{R,z} = \frac{\tau_B}{4\pi \; R_0 \; B_0} \; \frac{\partial \Psi}{\partial z_B} \tag{9}$$

2.3 Interaction with ICRH electro-magnetic field.

In order to make possible the modeling of the high energy minority ions produced in the JET plasma by ICRH heating a simple ICRH operator L_{RF} (f) has been added to the right hand side of equation 1. In its simplest form, neglecting effects of a finite parallel wave number, L_{RF}(f) can be written as [11]:

$$L_{RF}(f) = \frac{1}{G_{RF}} \; \frac{\partial}{\partial v_{\perp,res}} \left(G_{RF} \; D_{RF} \frac{\partial f}{\partial v_{\perp,res}} \right) \tag{10}$$

Here we use the coordinates $v_{\perp,res}$ and $v_{//,res}$, the perpendicular and parallel velocity at the resonance location. The RF acceleration affects to first order only $v_\perp$, while leaving $v_{//}$ unaffected. The ICRH diffusion operator is then written as:

$$D_{RF} = \frac{1}{\tau_B \; v_{//,res}} \; K_{RF} \; \left| J_{H-1}\left(\frac{k_\perp \; v_{\perp,res}}{\omega_{ci}}\right) + \frac{E_-}{E_+} \; J_{H+1}\left(\frac{k_\perp \; v_{\perp,res}}{\omega_{ci}}\right) \right|^2 \tag{11}$$

where K_{RF} is a multiplier for the ICRH power, J_H is the Bessel function of order H, H is the harmonic number, E_- and E_+ are the left and right handed

polarisation components of the ICRH (fast wave) field, $k_\perp$ is the perpendicular wave-number and ω_{ci} is the ion cyclotron angular frequency at the resonance.

The Jacobian for the coordinates is:

$$G_{RF} = G_{v,a,\lambda} \quad \frac{B_0}{B_{res}} \quad \frac{v_{//,res} \quad v_{\perp,res}}{v^3} \tag{12}$$

where B_{res} is the magnetic field at the resonance radius.

There is a particular difficulty in applying this type of operator in a Monte Carlo code, because it is not a priori known how much power will be coupled to a distribution of particles in a given time step. This depends, namely, on the details of the random orbits. The problem is solved, both in general Fokker Planck applications of ICRH operators and in this code, by using a feedback scheme for the power multiplier K_{RF}, in which K_{RF} is determined on the basis of the power coupled in the previous time step.

A second consideration applies to the conservation of the minority density under particle loss. In the Monte Carlo algorithm, this is ensured by seeding a new particle, at low energy, for every particle that is lost. The seeding is such that a minority density profile in normalised minor radius a is approximately conserved, and is random in pitch angle parameter λ.

2.4 Statistical approach to the solution of the FP equation.

In Monte Carlo methods the solution of a partial differential equation is replaced by the numerical calculation of random motion of a large number of test particles. In this section, following [12], we show the derivation of the Langevin equations for the advancement of particle coordinates in time. We consider here only the case of one-dimensional operators, taking advantage of the fact that each of the specific operators used in this paper can be written so as to affect only one coordinate. The corresponding multi-dimensional case is discussed in [13].

Equation 1 can be rewritten in the following general form:

$$\begin{aligned} &\frac{\partial f}{\partial t} + \frac{1}{G} \frac{\partial}{\partial x} (G \ \Phi) = S \\ &\Phi = Uf - D \frac{\partial f}{\partial x} \end{aligned} \tag{13}$$

where x is a generalised coordinate, G is a jacobian, Φ is a generalised flux, of which U is a convective term and D is a diffusion coefficient, and S is a source.

We introduce the first and second moments of the distribution function, defined as the average position $< x > = \int x \; G \; f \; dx$, and the distribution width $\sigma = < (x - < x >)^2 > = \int (x - < x >)^2 \; G \; f \; dx$.

To derive the Langevin equation, we consider the time evolution of these moments for an initial distribution of test particles which at t = 0 all have the same value of the coordinate $x = x_0$, i.e. $f(t = 0) = (1 / G) \, \delta(x - x_0)$. Calculating the moments after a time Δt, with $f(\Delta t) = f(0) + \Delta t \; (\partial f / \partial t)$, and substiting the initial distribution, yields at $t = \Delta t$:

$$< x >_{\Delta t} = x_0 + \left(U + \frac{1}{G} \frac{\partial}{\partial x} (G \; U) \right) \Delta t \tag{14}$$

$$\sigma_{\Delta t} = 2 \; D \; \Delta t \tag{15}$$

We see that the average velocity of the test particles has two components, the first of which originates from the convective velocity U of equation 13 and the second of which represents a compensation of the gradient of the diffusive operator G D. The distribution at Δt is a Gaussian:

$$f(\Delta t) = \frac{1}{\sqrt{4 \; D \; \Delta t}} \exp\left(\frac{- (x - < x >)^2}{4 \; D \; \Delta t} \right) \tag{16}$$

The simplest way to generate this probability distribution for a test particle at time $t + \Delta t$, given the test particle coordinate at time t, is to use finite difference equation for the particle coordinate x as follows:

$$\begin{aligned} x(t + \Delta t) &= x(t) + V \Delta t \pm \sqrt{2 \; D} \\ V &= U + \frac{1}{G} \frac{\partial}{\partial x} (G \; D) \end{aligned} \tag{17}$$

where $\pm$ stands for a random choice of sign.

Now returning to the actual application we can write the equations for the advancement in time of the particle coordinates in the processes of slowing down, pitch angle scattering, ripple diffusion and ICRH acceleration as follows:

$$t_{n+1} = t_n + \Delta t$$

$$v_{n+1} = v_n - U_{slo}\ \Delta t$$

$$\lambda_{n+1} = \lambda_n + \frac{1}{G_{v,a,\lambda}} \frac{\partial}{\partial \lambda} \left(G_{v,a,\lambda}\ D_{pas} \right) \Delta t \pm \sqrt{2\ D_{pas}\ \Delta t}$$

$$z_{B,n+1} = z_{B,n} + \frac{1}{G_{R,z}} \frac{\partial}{\partial z_B} \left(G_{r,z}\ D_{rip} \right) \Delta t \pm \sqrt{2\ D_{rip}\ \Delta t}$$

$$v_{\perp,res,n+1} = v_{\perp,res,n} + \frac{1}{G_{RF}} \frac{\partial}{\partial v_{\perp,res}} \left(G_{RF}\ D_{RF} \right) \Delta t \pm \sqrt{2\ D_{RF}\ \Delta t}$$

These operations are applied in sequence, with the necessary coordinate transformations carried out in between.

2.5 Implementation in the RLX-1 code.

The approach described above has been implemented in the numerical code RLX -1. The code has a pre-processing part which provides the necessary averaging over the particle orbits for a given plasma equilibrium and generates 1D and 2D maps of all coefficients in the FP equation (τ_s, F, Δz, Jacobians, etc.). These maps are used in the main part of the code, which calculate the evolution of a large number of particle random orbits. The structure of the code makes it possible to model time-dependent scenarios of plasma parameters and particle sources. The code treats the processes of slowing down, pitch angle scattering, collisional and stochastic ripple diffusion, ICRH acceleration, first orbit loss for trapped particles, loss due to ripple well trapping, and loss due to ripple diffusion. Initial distributions, or source distributions can be specified. Optionally, a full neutral beam source can be included using an interface with a neutral beam deposition code. The code also incorporates a model for particle re-distribution during a sawtooth crash.

In the framework of the statistical treatment the sawtooth redistribution is straightforward. At the time of the sawtooth crash, all test particles which lie inside a given minor radius, the sawtooth mixing radius, have their minor radii changed randomly within a distribution given by the relevant jacobian, under conservation of the particle energy and magnetic moment. This procedure provides uniform density profile inside the mixing radius after the sawtooth.

3. BENCHMARKING WITH A FULL ORBIT FOLLOWING MONTE-CARLO CODE

The code RLX-1 has been benchmarked by a comparison with the full OFMC DRIFT, developed at the I.V.Kurchatov Institute for analysis of alpha-particle ripple loss in ITER CDA [3]. The benchmark calculations have been made for plasma profiles and magnetic field configuration corresponding to JET pulse #27076, with 16 toroidal field coils. The plasma is in an an up-down symmetric inner-wall configuration with a plasma current of I = 2.5MA and a toroidal magnetic field in the plasma centre (R_0 = 3 m) of B = 1.4T. The map of the ripple amplitude δ is shown in Fig.1.

In section 3.1 some general observations are made on the drift surfaces, as examined with the DRIFT code. In section 3.2 the validity of the analytical expression describing transport in this drift surface structure is discussed, on the basis of a comparison of particle cloud spreading between the RLX-1 and DRIFT codes. In section 3.3 local loss fractions for high energy particles, as obtained with the two codes, are compared. In section 3.4 the ICRH operator results are compared with an analytical prediction, i.e. the "Stix tail".

3.1 Structure of drift surfaces in the presence of TF ripple

Stochastic diffusion in a rippled toroidal field originates from the distortion of the drift surfaces. The structure of banana particle drift surfaces in the case of 16 TF coils has been studied with the DRIFT code.

The conservation of particle energy and magnetic moment constrain the banana tip motion to surfaces with B = const, which are close to surfaces with R = const. Therefore the drift surfaces can be represented in the (z_B,φ_B) plane Z_b,φ_b , where z_B is the vertical co-ordinate and φ_B is the toroidal co-ordinate of the banana tip position ($v_{||}$ = 0). Because of the toroidal drift and ripple displacements, the banana tip jumps to another point in the Z_b,φ_b plane after each bounce period. The sequence of the tip positions constitute a Poincare map for a drift surface.

Fig.2a shows the drift surfaces of protons with energy E = 0.28 MeV started from R_B = 3.0 m , φ_B = 0 and different vertical positions of the banana tip. These protons have the same orbits as 0.14MeV deuterium ions produced by neutral beam injection in JET . The Poincare maps were calculated by the DRIFT code

with Coulomb collisions switched off, and consist of 200 bounces for each particle. It can be seen that the region with "good" drift surfaces ($0.4 < z_B < 0.9$), which are only slightly distorted by the ripple, is surrounded at both sides by island structures located near resonance surfaces. Above $z_B = 1.2$ m the drift surfaces are mainly destroyed - only small islands of stability still exists. Above $z_B = 1.4$ m it takes only few bounce periods for particle to be trapped in the ripple well and lost. There is always another stochastic region near equatorial plane (below $z_B = 0.2$ m at Fig.2a).

An increase of particle energy does not change drastically the structure of the drift surfaces. As shown in figure 2b and 2c, the position of resonant surfaces does not move significantly when the particle energy increases up to 1 MeV. The main effect is the further destruction of drift surfaces near the islands.

3.2 Numerical experiments with clouds of test particles

The analytical expression for the diffusion rate, as given in equations 4 and 5, was checked for JET parameters by comparison with the diffusion rate derived from the results of the DRIFT code. In the latter case the numerical diffusion rate was found from spatial spreading of a cloud of particles started from the same initial conditions. Because of the large consumption of the computer run time we could compare only a limited number of points in the plasma cross section. The clouds, which consisted of 500 particle, were advanced in time about $2\ 10^{-3}$s.

Figure 3 shows as an example of the time evolution of the second moment of a 1 MeV proton cloud starting initially from the point $R_B = 3$m, $z_B = 0.7$m (coordinates of banana tip positions) which is located in the region with well conserved drift surfaces (see Fig.2). It can be seen that an initial ballistic spreading of the cloud is followed by a spreading of a diffusive type at $t = 10^{-4}$s. The ripple diffusion in this point is very small, of order $D = 0.04$ m^2/s. Figure 4 shows the distribution of the banana tip positions over the vertical coordinate after $t = 2\ 10^{-3}$s. The two curves in figure 4 have been obtained for the same cloud by the RLX-1 and DRIFT codes. It can be seen that this particular point the distributions are very similar.

Figure 5 shows the diffusion rate as function of the vertical coordinate of the banana tips for 1 MeV protons at $R_B = 3.0$m. The solid lines represent analytic formulas, Eq.4 and Eq.5, crosses with error-bars are the data obtained from

numerical experiments with the DRIFT code. The horizontal error bars on the DRIFT results arise from the finite width of the cloud. Large vertical error bars at large and small z_B are associated with banana particle loss (at low z_B banana particles transfer to transit particles). Closer to the ripple well boundary, particle spreading cannot be described in terms of diffusion because a large fraction of the particles is lost during the ballistic regime. However the large diffusion rate given by equations 4 and 5 near the ripple well boundary also result in very short confinement times, in comparison with the particle slowing down time, and one can expect a reasonably good description of the total loss fraction on the basis of equations 4 and 5.

3.3 Comparison of local loss fractions.

A comparison of ripple loss fractions, between RLX-1 and DRIFT, was performed for fast tritons produced by D-D fusion reactions. Such tritons have a birth energy of 1MeV and the width of the banana orbits is therefore large. Owing to this, the comparison provides a test of the applicability of the RLX-1 code, in which zero banana width is assumed.

In order to carry out this comparison, RLX-1 was modified to include first orbit loss for trapped particles, as this is a significant loss channel for tritons. With both codes, local loss fractions were calculated for a number of flux surfaces. The slowing down history of tritons launched from an isotropic source located on a flux surface was followed until either the particle was lost or it had slowed down to below a cut-off energy.

In the calculations with RLX-1, a thousand particles were.launched on each of ten uniformly spaced flux surfaces. The cut-off energy was chosen as 20keV. All loss channels described above were included. In the DRIFT calculations, one hundred particles were launched per flux surface, and the cut-off energy was set to 100keV. In DRIFT, particles are considered lost if they come closer to the wall then a toroidal larmor radius.

Figure 6 shows a comparison of the local loss fractions. As can be seen, the results are fairly close to each other, with DRIFT predicting slightly larger losses. Thus, equations 4 and 5 give a satisfactory description of ripple-induced losses in the JET 16 coil geometry, even when the fast ions have large banana width. This conclusion is consistent with the findings in [15], where the influence of finite

orbit width on the Chirikov parameter γ was studied. It was found in [15] that, although γ can be significantly affected by finite orbit width effects, the number of stochastically moving particles is only marginally affected. The main reason for this are the steep ripple diffusion coefficient gradients in the JET experiment, i.e. the region over which the transition from $\gamma << 1$ to $\gamma > 1$ takes place is small. Furthermore, for particles in regions with $\gamma > 1$, the loss occurs on a time scale which is much faster then a slowing down time. Consequently, the details of the ripple diffusion coefficient are not very important for the determination of the loss fraction (this observation is also the basis for the treatment in the RIPLOS [5] code, see introduction).

3.4 Test of the ICRF operator

In order to check if the Monte-Carlo ICRH operator gives reasonable results, the following test case has been used. A calculation was performed for fundamental minority heating of protons, with $P\ \tau_s / N = 3.10^6$eV, where P is the ICRH power, τ_s the slowing down time and N the number of Monte-Carlo particles absorbing the power (N = 5000). There is no radial convection or diffusion, i.e. all the protons are located on a single flux surface at r/a = 0.3.

Under these circumstances the averaged energy of the protons in the tail of the velocity distribution should correspond to a Stix "temperature" [16] of 1 MeV. Figure 7 shows the comparison of the velocity distribution calculated by the RLX - 1 code and a 1 MeV tail distribution. As can be seen the agreement is good, demonstrating the validity of the ICRH Monte-Carlo operator.

4. NUMERICAL SIMULATION OF THE RIPPLE LOSS OF FAST PARTICLES IN JET.

The newly developed code has been used for modelling of fast particle losses in the JET experiment with 16 versus 32 TF coils [6,7]. Here we present some results of the modelling of NBI particles and ICRH minority ions in the discharges with enlarged TF ripple.

4.1 Ripple loss of neutral beam ions.

The NB injection provides fast deuterium ions with a maximum energy of 140 keV. In the modelling the full magnetic geometry is considered and full a

NBI source was used, including injection geometry and fractional energy components. Temperature and density profiles and time evolution of plasma parameters correspond to those measured experimentally in shot #27076, with a toroidal field of 1.4T, plasma current 2.5MA, and inner-wall configuration.

Calculated particle and energy losses and losses of electron and ion heating powers are shown in Table 1 for different loss channels. The losses have been calculated by slowing down of 4790 test particles which corresponds to 100% in Table 1.

Energy and particle fractions	No loss cone. No ripple diffusion	Loss cone. No ripple diffusion	Loss cone. Collisional diffusion	Loss cone. Collisional plus stochastic diffusion
to electrons	55%	50%	49%	48%
to ions	45%	40%	39%	39%
lost	0%	10%	12%	13%
particles lost	0%	26%	31%	31%

Table 1. Energy and particle loss fraction for NBI.

In column 2 we consider the 'no loss' case, in which both ripple well trapping losses and ripple diffusion operator are switched off. In columns 3,4,5, the ripple well losses are switched on. The ripple diffusion operator is switched off in column 3, represents only collisional ripple diffusion in column 4, and represents collisional plus stochastic diffusion in column 5.

It can be seen that the main loss mechanism for the NB ions is via the ripple well trapping. This includes NBI directly into the loss cone plus pitch angle scattering. Collisional ripple diffusion adds about 2% to ripple loss, while stochastic diffusion adds about 1%.

Because of a relatively low magnetic field in the experiments with TF ripple, B = 1.4 T, the sawtooth inversion radius is large, r = 0.75m, and the time traces of the central plasma parameters including the neutron rate display significant sawtooth oscillations. This indicate a possible redistribution of beam particles

during sawtooth crashes. The next series of calculations has been done to analyse possible effect of sawteeth on the ripple loss of NBI particles. In the numerical modelling of the sawtooth effect a source of NBI particles has been switched on for 1.5s. Ripple well loss and ripple diffusion operators are switched on. Sawteeth were introduced at t = 0.1, 0.3, 0.5, 0.7, 0.9, 1.1, 1.3 s and all particles inside the a mixing radius V_{mix} are redistributed as described above. Table 2 shows the data for particle and power losses at t = 1.5 s when steady state was established, for various values of the mixing radius. The first column corresponds to the case without sawteeth (slightly different plasma conditions give a slightly higher loss and slightly different electron/ion heating distribution than the corresponding case in table 1 (14.6 versus 13%).

Power fraction	No sawteeth	Mixing radius r_{mix} / a = 0.75	Mixing radius r_{mix} / a = 0.9
To electrons	43	43	43
To ions	42	41	39
Lost	14.6	16.2	18.4

Table 2. Effect of sawteeth on the power loss of NBI particles.

It can be seen that sawtooth effects does not significantly change the ripple losses , even at very large inversion radii. This result has the following interpretation. Because of the conservation of the particle magnetic moment and energy, the particle banana tip stays on the same major radius during the particle redistribution in a sawtooth crash and thus the distance between banana tip position and ripple well boundary remains approximately the same. As a result the confinement time of the particle, defined mainly by particle scattering to the ripple well loss cone, does not change significantly. In addition, the original NBI deposition profile is rather flat, so that the redistribution does not make a big difference to it.

In comparing the results of the simulation with the experimentally observed loss of plasma stored energy in the 16 coil discharges, account should be taken of two effects: first, the loss os NBI particles and power due to ripple and second, the effect of ripple on the thermal energy confinement. Taking into account these two processes, we find that the calculated loss is smaler than the experimental loss [17]. Based on the observation of lower ion temperatures in the ohmic phases

of the 16 coil discharges, it is postulated in [17] that primarily an additional effect of the ripple on the thermal energy confinement is resonsible for the discrepancy.

4.2 ICRH accelerated fast ions.

In order to explore losses of particles with higher energies than NBI, ICRH fast wave minority heating was used to produce high energy protons.. The concentration of protons was kept low in order to obtain a minority tail with energy up to the MeV range. As a consequence of the low toridal field, the second harmonic of the ion cyclotron frequency was used. As far as studying ripple losses is concerned, ICRH accelerated ions have the advantage that first, most energetic ions are banana-trapped and second, that their turning point major radii R_B tend to be located close to the resonance. By moving the cyclotron resonance, an insight into the dependence of the ripple transport on the major radius of the turning point can be gained. The effect of the ripple on the fast protons was therefore explored experimentally by scanning the resonance location from the high to the low field side.

The relative ICRH heating efficiency for 16 versus 32 coils is defined as $\eta = (\Delta W_{dia} / P_{ICRH})_{16} / (\Delta W_{dia} / P_{ICRH})_{32}$., with W_{dia} the diamagnetic plasma energy This quantity is shown in figure 8 as a function of ICRH resonance location (solid triangles). Clearly, the relative heating efficiency is strongly reduced as the resonance is moved towards the LFS of the machine, where we note that the resonance at 3.34m is not, and the resonance at 3.76m is, in the ripple well region.

This loss of heating efficiency has been modelled with the RLX-1 code and compared with experimental results. The result of the comparison are also shown in figure 8 (solid circles). An additional loss of 25% due to thermal effects has been added to the calculated loss, consistent with the findings in the NBI case [17]. For reference, the NBI case relative heating efficiency is also indicated.

We conclude from the figure that there is a reasonable agreement between the simulations and the experimental results. The loss of heating efficiency calculated by the RLX-1 code tend to be somewhat less than the experimental one, but is within about a factor 2. There can be number of reasons for this. One problem in the simulations is that no reliable measurements of the hydrogen concentration are available. In the calculations presented here a concentration of

5% has been assumed. A lower concentration would lead to more energetic tail ions and therefore to more losses due to stochastic diffusion. Other effects, such as RF-induced spatial diffusion and additional convection and diffusion due to neo-classical effects might play a role . It is difficult to assess the influence of such effects at present.

It is important to find out how much stochastic diffusion contributes to the losses in the simulations. In order to do this the code has been run with the stochastic diffusion switched off but with ripple well trapping kept. For the case with the resonance at 3.34m (and for all smaller R_{res}) no significant loss of heating efficiency is seen without stochastic diffusion. This identifies stochastic diffusion as the primary loss channel for the ICRH minority ions.

5. CONCLUSIONS

The new RLX-1 code, based on a Monte-Carlo solution of the bounce average FP equation, is a powerful tool for modelling of ripple losses of fast particles. The code has been benchmarked against a full orbit following Monte-Carlo code. A good agreement between the two codes was found, indicating that the analytic expression for the ripple diffusion given in reference [6] give an adequate description of ripple losses of fast particles for the JET configuration and ripple profiles.

The analysis of JET NBI discharges with enhanced TF ripple showed that the main loss mechanism for 140keV NBI particles is pitch-angle scattering into the ripple well region. Other loss mechanisms such as stochastic diffusion and first orbit losses only play a minor role. On the other hand, stochastic diffusion was found to be the primary loss mechanism for MeV range minority ions accelerated by ICRH. This is particularly clear when the cyclotron resonance is located off axis in regions with significant ripple, but still outside the ripple well region.

The comparison of the results from the numerical modelling with the experimental ripple losses show that in general the experimental losses are somewhat larger than the predicted ones. The postulate is made in [17] that primarily enhanced ripple losses of the bulk thermal plasma are responsible for this discrepancy. Under this postulate, the experimental results on fast particle losses can be explained within the framework of the existing theory.

REFERENCES

[1] TANI, K., TAKIZUKA, T., AZUMI, M.H., Nucl Fusion **23** (1983) 657.

[2] HIVELY, L.M., ROME, J.A., Nucl Fusion **30** (1990) 1129.

[3] KONOVALOV, S.V., PUTVINSKII, S.V., SAPLAHYDI, A.V., SMIRNOV, A.P., Report ITER-IL-9-Ph-S1, 1989.

[4] ZAJTSEV, F.S., SMIRNOV, A.P., YUSHMANOV, P.N., Nucl Fusion **26** (1986) 1311.

[5] WHITE, R.B., BOOZER, A.H., GOLDSTON, R.J., et al, Plasma Phys and Contr. Nucl Fus Research, IAEA, Vienna 1982, **3**, 391.

[6] SADLER, G., BARABASCHI, P., BERTOLINI, E., et al., Plasma Phys. and Contr. Fusion, V.34, N13 (1992) 1971.

[7] TUBBING, B.J.D., and JET Team, in proc. of IAEA Conf. on Plasma Phys. and Contr. Nucl. Fusion Research, Würzburg, Germany, 1992, IAEA- CN-56/A-7.5.

[8] YUSHMANOV P.N., Review of plasma physics, **16** edited by B.B.Kadomtsev (Consultants Bureau, New York) 117.

[9] FRIEMAN, E.A., Phys Fluids, **13** (1970) 490.

[10] GOLDSTON, R.J., TOWNER, H.H., J.Plasma Phys. **26** (1981) 283.

[11] ANDERSON, D., LISAK, M., PEKKARI, L.O., Phys. Fluids **28** (1985) 3590

[12] BOOZER, A.H., KUO-PETROVICH, G., Phys Fluids **24** (1981) 851.

[13] PUTVINSKII S.V., TUBBING B.J.D., JET report JET-R(93)03.

[14] GOLDSTON, R.J., WHITE, R.B., BOOZER, A.H., Phys. Rev. Lett. **47** (1981) 647.

[15] ERIKSSON, L.G., HELANDER, P., Nuclear Fusion, **33** (1993) 767.

[16] STIX, T.H., Nucl. Fusion, **15** (1975) 737.

[17] TUBBING, B.J.D., and JET Team, Europhysics conference abstracts 17C-1 (1993) 39.

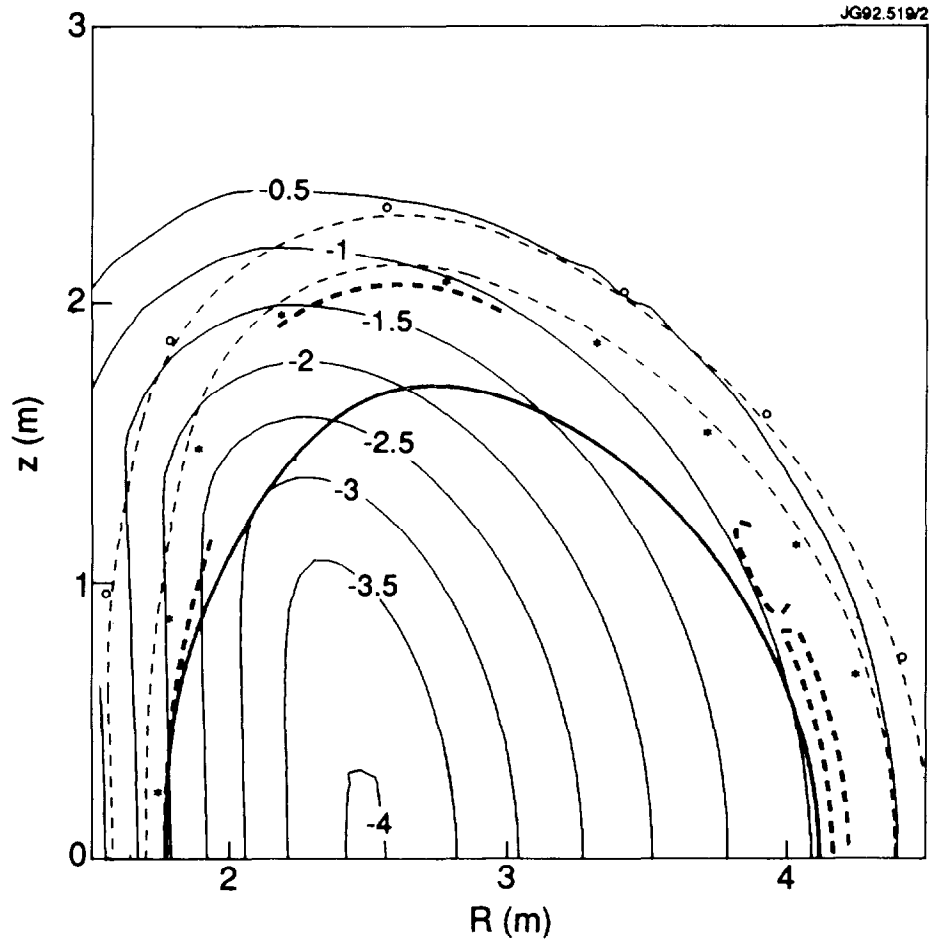

Figure 1: Contours of ripple value $\delta = (B_{max} - B_{min})/(B_{max} + B_{min})$ and plasma boundary, for JET discharge 27076 with 16 TF coils.and $I_p = 2.5$ MA. $B_t = 1.4$T.

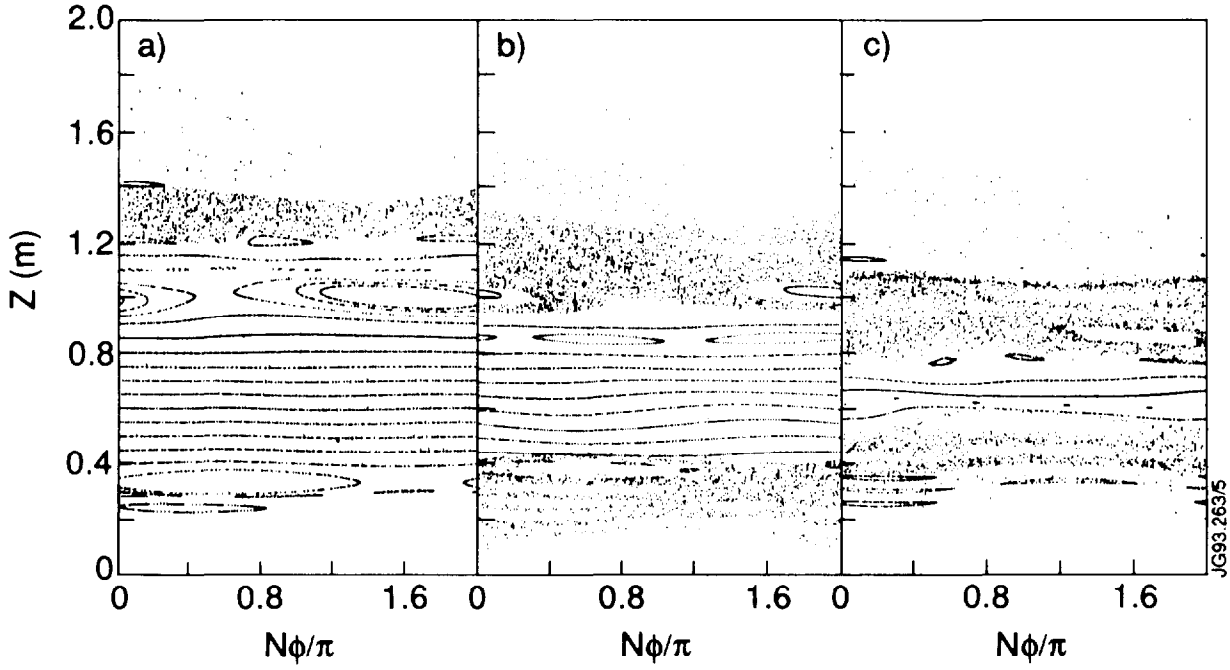

Figure 2: Poincaire map for drift surfaces of banana-trapped protons with different energies.

a E = 0.28 MeV (equivalent to NBI ions of 140 KeV in JET).

b E = 1 MeV (typical energy for ICRH minority).

c E = 3 MeV (equivalent to DD tritons).

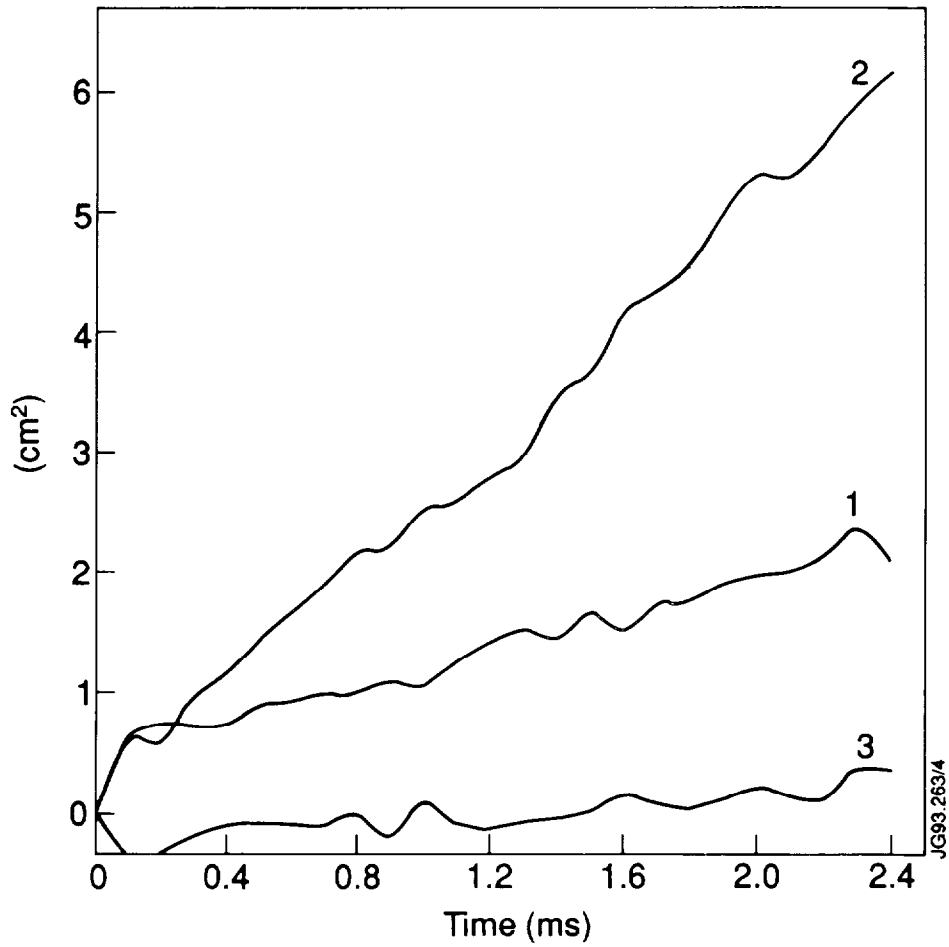

Figure 3: Second moments as function of time for a proton cloud starting from R_B = 3.0 m, z_B = 0.7 m. Energy is 1 MeV.

1 - $\langle (Z-\langle Z\rangle)^2 \rangle$.

2 - $\langle (R-\langle R\rangle)^2 \rangle$.

3 - $\langle (Z-\langle Z\rangle)(R-\langle R\rangle)\rangle$.

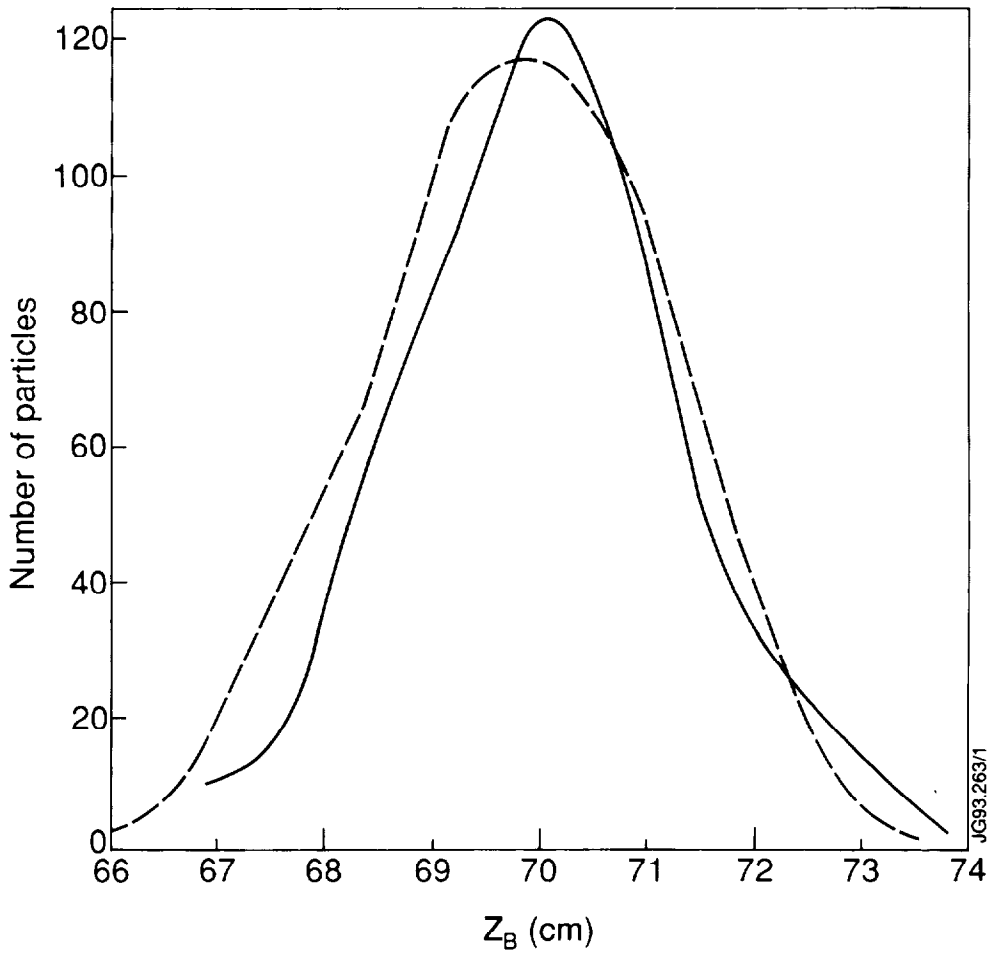

Figure 4: Distribution of particles in the cloud after 2ms. Starting point is R_B = 3.0m, z_B = 0.7m. Energy is 1MeV. Dashed line, OFMC DRIFT; Solid line, the RLX-1 code.

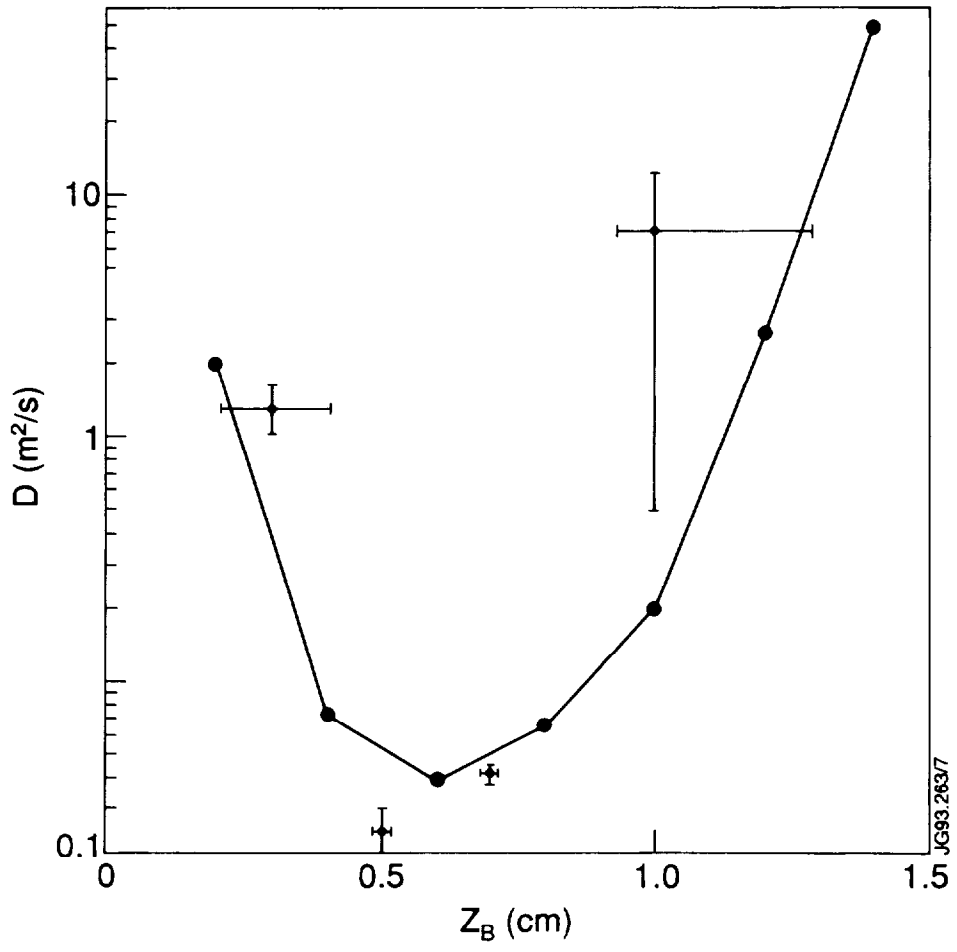

Figure 5: Diffusion rate versus vertical coordinate of banana tip, for protons with energy of 1 MeV and R_B = 3.0m. Solid line, from equations.12 to 14; Dots with error bars, diffusion rate found from particle cloud spreading calculated by DRIFT.

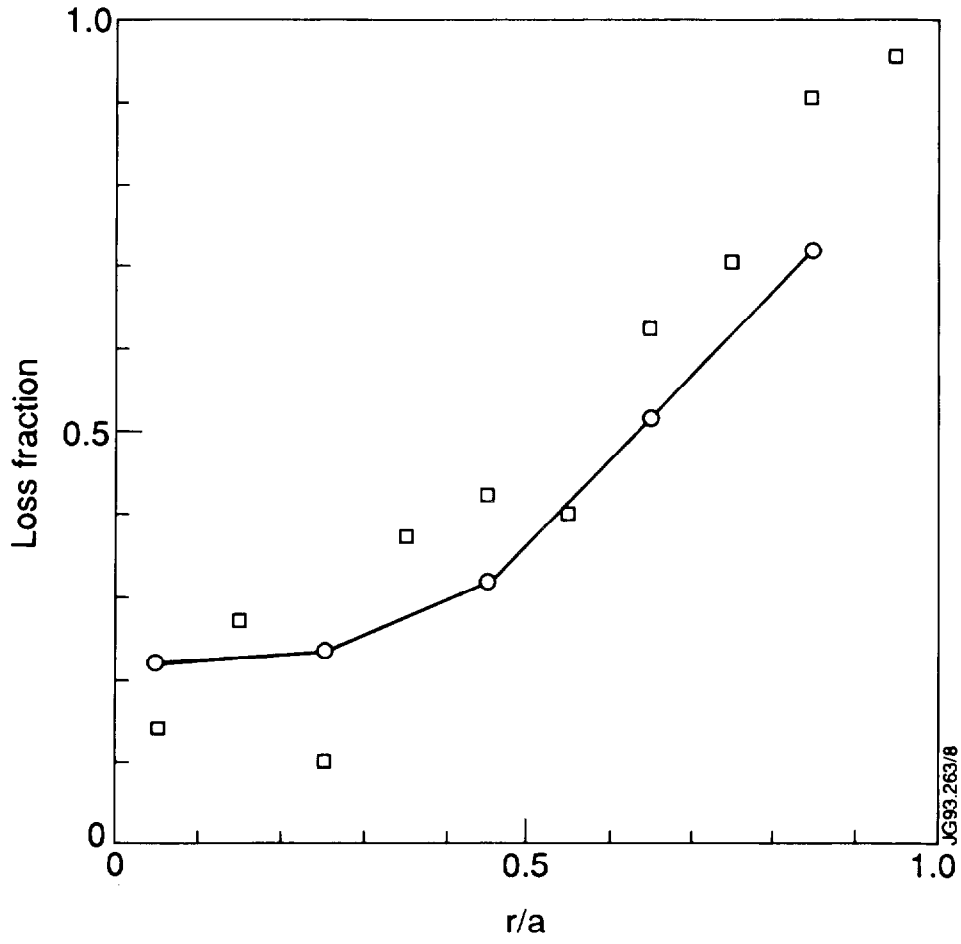

Figure 6: Local particle loss fraction of tritons with an initial energy of E = 1 MeV, as function of the normalised minor radius. Solid line as calculated by the RLX-1 code, open squares as calculated by DRIFT.

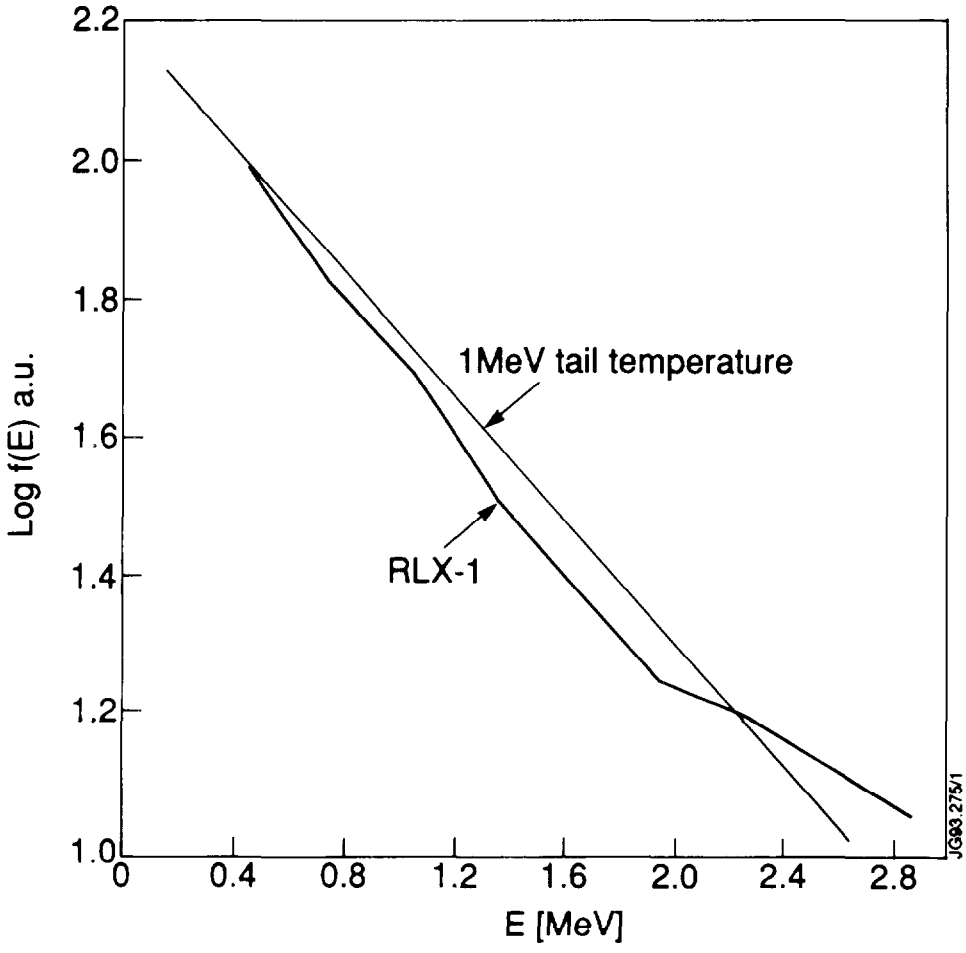

Figure 7: Energy distribution of minority ions heated by ICRH, as calculated by RLX-1. For reference, the Stix tail temperature is shown.

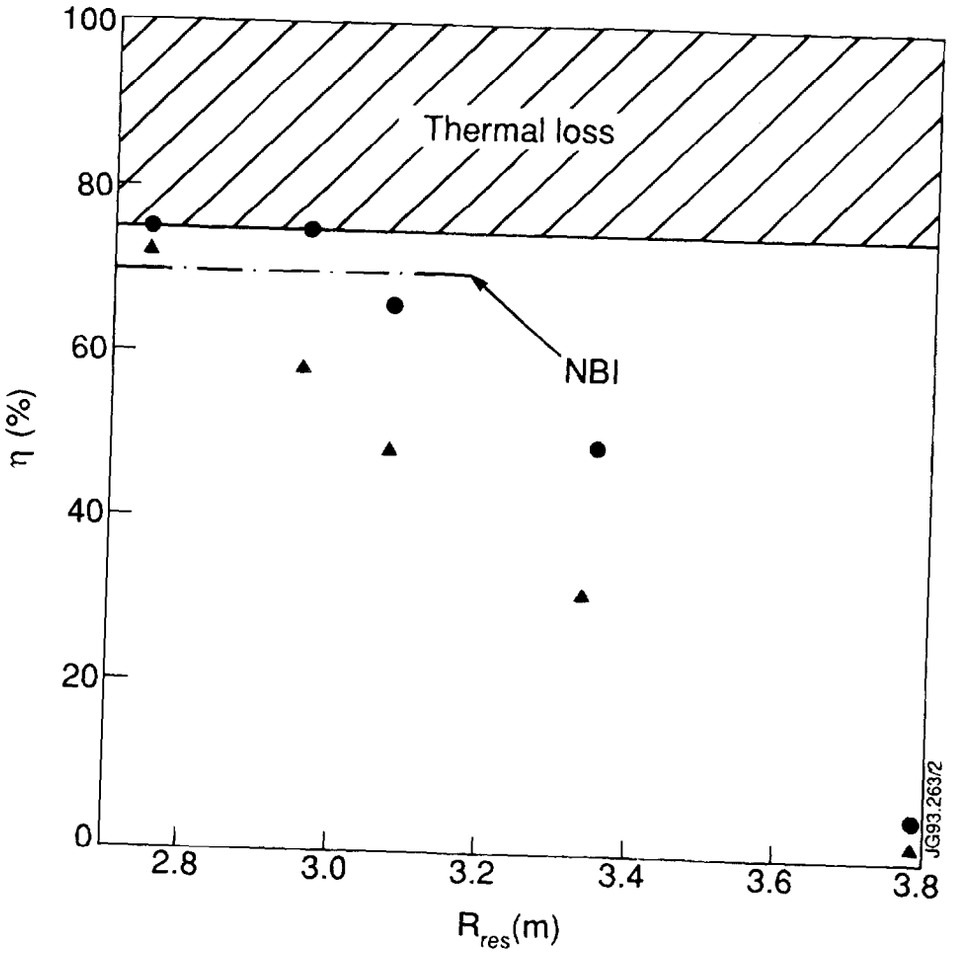

Figure 8: Ratio of heating efficiency for 16 and 32 coils as a function of resonace location for discharges with ICRH. Shaded area; postulated loss due to thermal plasma loss. Triangles, experimental results; circles, numerical modelling, including a 25% thermal loss contribution.